

TWO MODELS FOR SURFACE SEGMENTATION USING THE TOTAL VARIATION OF THE NORMAL VECTOR

LUKAS BAUMGÄRTNER, RONNY BERGMANN, ROLAND HERZOG,
STEPHAN SCHMIDT, AND MANUEL WEISS

ABSTRACT. We consider the problem of surface segmentation, where the goal is to partition a surface represented by a triangular mesh. The segmentation is based on the similarity of the normal vector field to a given set of label vectors. We propose a variational approach and compare two different regularizers, both based on a total variation measure. The first regularizer penalizes the total variation of the assignment function directly, while the second regularizer penalizes the total variation in the label space. In order to solve the resulting optimization problems, we use variations of the split Bregman (ADMM) iteration adapted to the problem at hand. While computationally more expensive, the second regularizer yields better results in our experiments, in particular it removes noise more reliably in regions of constant curvature.

1. INTRODUCTION

Segmentation of surfaces is a fundamental task in computer vision and shape analysis. Its goal is to partition a given surface into disjoint regions based on some features. In this paper, we consider surfaces that are represented by a mesh Γ consisting of a set \mathcal{T} of triangles and a set \mathcal{E} of edges in \mathbb{R}^3 . As the feature, we use the piecewise constant unit outer normal vector field \mathbf{n} of the surface. Segmentation then becomes the task of assigning a label to each triangle $T \in \mathcal{T}$, based on a measure of similarity of the normal vector to a set of prescribed label vectors $\mathbf{g}_1, \dots, \mathbf{g}_L$ belonging to the unit sphere $\mathcal{S} := \{\mathbf{x} \in \mathbb{R}^3 \mid |\mathbf{x}|_2 = 1\}$.

The result of a segmentation is expressed in terms of an assignment function $\varphi: \mathcal{T} \rightarrow \Delta$. The value φ_T on each triangle T belongs to the probability simplex $\Delta := \{\mathbf{x} \in \mathbb{R}^L \mid \mathbf{1}^T \mathbf{x} = 1, \mathbf{x} \geq \mathbf{0}\}$. The label assigned to a triangle T will be the one associated with the dominating entry of the assignment function, i.e., $\ell_T^* = \arg \max_{\ell} \varphi_{T,\ell}$.

We follow a classical variational approach by minimizing a fidelity term that measures the similarity $s_{\ell}(\mathbf{n})$ of the normal vector \mathbf{n} to any of the label vectors \mathbf{g}_{ℓ} . We employ the geodesic distance on the sphere \mathcal{S} for this purpose, i.e., we set $s_{\ell}(\mathbf{n}) := d(\mathbf{n}, \mathbf{g}_{\ell})$. These values can be pre-computed. We obtain the problem

$$(1.1) \quad \underset{\varphi: \mathcal{T} \rightarrow \Delta}{\text{Minimize}} \quad \sum_{T \in \mathcal{T}} |T| \sum_{\ell=1}^L s_{\ell}(\mathbf{n}_T) \varphi_{T,\ell} + \beta \mathcal{R}(\varphi).$$

2010 *Mathematics Subject Classification.* 65D18, 68U10, 49M29, 65K05, 90C30.

Key words and phrases. total variation, surface segmentation, non-smooth optimization, ADMM.

This work was supported by DFG grants HE 6077/10-2 and SCHM 3248/2-2 within the Priority Program SPP 1962 (Non-smooth and Complementarity-based Distributed Parameter Systems: Simulation and Hierarchical Optimization), which is gratefully acknowledged.

Here, $|T|$ denotes the area of T , $\beta > 0$ is a regularization parameter and \mathcal{R} is a regularizing functional.

The goal of this paper is to compare two regularization approaches, one of which is new in surface segmentation problems.

The first regularizer was originally proposed for image segmentation problems in [Lellmann, Kappes, et al., 2009](#) and further developed in [Lellmann, Schnörr, 2011](#); [He et al., 2012](#). This regularizer measures the total variation of the assignment function φ in the assignment simplex Δ , and thus we refer to it as *assignment space total variation*, or A-TV in short. The variational problem (1.1) at hand has the same structure as in [Lellmann, Kappes, et al., 2009](#), but the pixels of the image domain are replaced by the triangles of the surface mesh and their color or gray-scale values are replaced by the normal.

A drawback of A-TV is that it does not incorporate any metric structure in the space of labels. Any transition between labels is penalized equally, regardless of the distance between the labels. We therefore propose an alternative regularizer, which measures the total variation in the label space \mathcal{S} instead. We refer to this new approach as *label space total variation*, or L-TV in short.

We expect that L-TV will allow for smoother assignments, e. g., in regions of constant curvature, where neighboring normal vectors are close to each other. On the other hand, L-TV is more involved computationally. On any given triangle T , the assignment function φ takes values in the simplex Δ . Any non-vertex point in the simplex corresponds to a mixed assignment. Since the labels reside in a nonlinear space (the sphere \mathcal{S}), a mixture of these labels is not simply a convex combination but rather a nonlinear weighted average known as the Riemannian center of mass; see [Karcher, 1977](#).

Let us briefly discuss alternative approaches to surface segmentation. The authors in [Hwan Kim, Dong Yun, Uk Lee, 2006](#); [Wang, Yu, 2011](#) use an approach that iteratively merges triangles into larger regions, which is also based on the outer normal vector field. Furthermore, [Sun, Harik, Baek, 2018](#); [Gauthier et al., 2017](#); [Yamauchi et al., 2005](#) compute an assignment based on the discrete curvature of the mesh, which is closely related to the normal vector \mathbf{n} . In an alternative variational approach, [Cohen-Steiner, Alliez, Desbrun, 2004](#); [Yan et al., 2012](#) minimize the distance of the original mesh to a mesh associated with the segmentation. The authors in [Nabi, Douik, 2016](#); [Zhang et al., 2012](#) propose to minimize the Mumford-Shah functional [Mumford, Shah, 1989](#), which is well-known from imaging.

Finally, there is also a stream of literature in geometric and topological data science, in which neural networks are trained to perform the task of surface segmentation or related inverse shape problems; see, e. g., [Hanocka et al., 2019](#); [Charles et al., 2017](#).

This paper is structured as follows: [Section 2](#) introduces the required notions on triangulated surfaces and differential geometry of the sphere \mathcal{S} and the probability simplex Δ . In [Section 3](#), we define the regularizers and discuss their differences. [Section 4](#) presents algorithms to solve the problems numerically. [Section 5](#) presents numerical results that allow A-TV to be compared to L-TV.

2. PRELIMINARIES

2.1. Discrete Surfaces. In this work, we consider triangulated surface meshes Γ that are embedded in \mathbb{R}^3 . We denote the set of triangles by \mathcal{T} and the set of edges

by \mathcal{E} . We work with manifold meshes without boundary, i. e., we assume that every edge E is connected to exactly two triangles. The two sides of an edge are denoted by E_+ and E_- , respectively, with arbitrary but fixed orientation. Furthermore, we assume that the surface is oriented, i. e., there exists a global outer unit normal vector field \mathbf{n} .

On the mesh Γ , we define the space of piecewise constant, X -valued functions

$$\mathcal{DG}(\mathcal{T}, X) := \{\mathbf{u}: \mathcal{T} \rightarrow X \mid \mathbf{u}|_T \in P_0(T, X) \text{ for all } T \in \mathcal{T}\}.$$

Here, $P_0(T, X)$ denotes the space of constant functions on the triangle T with values in X . On the skeleton (the union of edges), we analogously define

$$\mathcal{DG}(\mathcal{E}, X) := \{\mathbf{u}: \mathcal{E} \rightarrow X \mid \mathbf{u}|_E \in P_0(E, X) \text{ for all } E \in \mathcal{E}\}.$$

For ease of notation, we will denote the constant value of \mathbf{u} on a triangle T by $\mathbf{u}_T := \mathbf{u}|_T$ for $\mathbf{u} \in \mathcal{DG}(\mathcal{T}, X)$. Analogously, we write $\mathbf{u}_E := \mathbf{u}|_E$ for $\mathbf{u} \in \mathcal{DG}(\mathcal{E}, X)$.

Denoting the unit sphere in \mathbb{R}^3 by \mathcal{S} , we can express the fact that the normal vector field is piecewise constant by $\mathbf{n} \in \mathcal{DG}(\mathcal{T}, \mathcal{S})$.

For functions $\mathbf{u} \in \mathcal{DG}(\mathcal{T}, X)$ with values in a metric space $(X, d_X(\cdot, \cdot))$, we define the *total variation* as in [Bergmann et al., 2020a](#); [Lellmann, Strekalovskiy, et al., 2013](#)

$$(2.1) \quad \text{TV}_X(\mathbf{u}) := \sum_{E \in \mathcal{E}} |E| d_X(\mathbf{u}_{E_+}, \mathbf{u}_{E_-}),$$

where $|E|$ is the length of the edge E . Of particular interest will be the sphere, i. e. $X = \mathcal{S}$. We consider its metric in the following section.

2.2. Differential Geometry on the Sphere. Given a point $\mathbf{m} \in \mathcal{S}$, we denote its tangent plane by $\mathcal{T}_\mathbf{m}\mathcal{S}$. The tangent bundle \mathcal{TS} is the disjoint union of all tangent planes, endowed with the smooth structure inherited from \mathcal{S} . We choose the Euclidean inner product from the embedding $\mathcal{T}_\mathbf{m}\mathcal{S} \subseteq \mathbb{R}^3$ as the Riemannian metric on \mathcal{S} , turning the sphere into a Riemannian manifold. We denote the norm of a tangent vector by $|\cdot|_2$. Given a point $\mathbf{m} \in \mathcal{S}$, the exponential map is

$$\exp_\mathbf{m}: \mathcal{T}_\mathbf{m}\mathcal{S} \rightarrow \mathcal{S}, \quad \mathbf{X} \mapsto \exp_\mathbf{m} \mathbf{X}.$$

$\exp_\mathbf{m}(\mathbf{X})$ yields the point on the sphere that is reached by following the geodesic starting at \mathbf{m} in direction \mathbf{X} for unit time. The inverse mapping $\log_\mathbf{m}$ is well-defined except on pairs of antipodal points. It satisfies

$$\exp_\mathbf{m}(\log_\mathbf{m}(\widetilde{\mathbf{m}})) = \widetilde{\mathbf{m}} \quad \text{for } \widetilde{\mathbf{m}} \neq -\mathbf{m}.$$

The parallel transport $P_{\widetilde{\mathbf{m}} \leftarrow \mathbf{m}}: \mathcal{T}_\mathbf{m}\mathcal{S} \rightarrow \mathcal{T}_{\widetilde{\mathbf{m}}}\mathcal{S}$ transports a tangent vector at \mathbf{m} to a tangent vector at $\widetilde{\mathbf{m}}$ along the unique shortest geodesic from \mathbf{m} to $\widetilde{\mathbf{m}} \neq -\mathbf{m}$. For the explicit representations of the exponential map and parallel transport, we refer the reader to the appendix of [Bergmann et al., 2020b](#) or [Boumal, 2023](#), Exercise 10.38.

The choice of the Riemannian metric, i. e., the family of inner products in the tangent spaces $\mathcal{T}_\mathbf{m}\mathcal{S}$, induces a notion of distance on \mathcal{S} . For two points $\widetilde{\mathbf{m}}, \mathbf{m} \in \mathcal{S}$, the geodesic distance agrees with the ‘‘great arc distance’’

$$(2.2) \quad d_\mathcal{S}(\widetilde{\mathbf{m}}, \mathbf{m}) = \arccos(\widetilde{\mathbf{m}} \cdot \mathbf{m}) = \sphericalangle(\widetilde{\mathbf{m}}, \mathbf{m}),$$

where $\sphericalangle(\widetilde{\mathbf{m}}, \mathbf{m})$ denotes the angle (arc-length). As on any Riemannian manifold, the geodesic distance is related to the logarithmic map via

$$(2.3) \quad d_{\mathcal{S}}(\widetilde{\mathbf{m}}, \mathbf{m}) = |\log_{\mathbf{m}}(\widetilde{\mathbf{m}})|_2,$$

whenever the latter is defined; see also [Goto, Sato, 2021](#). The logarithmic map on the sphere \mathcal{S} is given by

$$(2.4) \quad \log_{\mathbf{m}}(\widetilde{\mathbf{m}}) = \begin{cases} \mathbf{0} & \text{if } \widetilde{\mathbf{m}} = \mathbf{m}, \\ \arccos(\widetilde{\mathbf{m}} \cdot \mathbf{m}) \frac{\widetilde{\mathbf{m}} - (\mathbf{m} \cdot \widetilde{\mathbf{m}}) \mathbf{m}}{|\widetilde{\mathbf{m}} - (\mathbf{m} \cdot \widetilde{\mathbf{m}}) \mathbf{m}|_2} & \text{otherwise,} \end{cases}$$

where again the case $\widetilde{\mathbf{m}} = -\mathbf{m}$ is excluded. It is worth noting that using (2.3) over (2.2) provides considerably more information about the structure of the non-smoothness of the problem. It is well known that $\widetilde{\mathbf{m}} \mapsto \log_{\mathbf{m}}(\widetilde{\mathbf{m}})$ is a smooth function in particular at $\widetilde{\mathbf{m}} = \mathbf{m}$. Hence the non-smoothness of (2.2) stems solely from the non-differentiability of the norm $|\cdot|_2$ at the tangent's space origin.

We further introduce the *Riemannian center of mass*, a generalization of the Euclidean mean on manifolds, as proposed by [Karcher, 1977](#). Given L points $\mathbf{g}_\ell \in \mathcal{S}$, $\ell = 1, \dots, L$ and corresponding weights $\varphi_\ell \in \mathbb{R}_{\geq 0}$, a point $\mathbf{m} \in \mathcal{S}$ is said to be a Riemannian center of mass w.r.t. the data $(\varphi_\ell, \mathbf{g}_\ell)$ if

$$(2.5) \quad \mathbf{m} \in \arg \min_{\mathbf{m} \in \mathcal{S}} \sum_{\ell=1}^L \varphi_\ell d_{\mathcal{S}}(\mathbf{m}, \mathbf{g}_\ell)^2.$$

In general, there is no closed-form solution to compute such \mathbf{m} . However, if a Riemannian center of mass \mathbf{m} fulfills $\mathbf{m} \neq -\mathbf{g}_\ell$ for all $\ell = 1, \dots, L$, the necessary optimality condition reads

$$(2.6) \quad 0 = \sum_{\ell=1}^L \varphi_\ell \log_{\mathbf{m}}(\mathbf{g}_\ell).$$

Notice that in Euclidean space, rather than the sphere, $\log_{\mathbf{m}}(\mathbf{g}_\ell) = \mathbf{g}_\ell - \mathbf{m}$ holds and thus (2.6) amounts to $\mathbf{m} = (\sum_{\ell=1}^L \varphi_\ell \mathbf{g}_\ell) / (\sum_{\ell=1}^L \varphi_\ell)$, thus explaining why the Riemannian center of mass generalizes the Euclidean mean.

For $\mathbf{m} \in \mathcal{DG}(\mathcal{T}, \mathcal{S})$, we further define

$$\begin{aligned} \mathcal{DG}(\mathcal{T}, \mathcal{TS}, \mathbf{m}) &:= \{\mathbf{Y} \in \mathcal{DG}(\mathcal{T}, \mathcal{TS}) \mid \mathbf{Y}_T \in \mathcal{T}_{\mathbf{m}_T} \mathcal{S} \text{ for all } T \in \mathcal{T}\}, \\ \mathcal{DG}(\mathcal{E}, \mathcal{TS}, \mathbf{m}) &:= \{\mathbf{X} \in \mathcal{DG}(\mathcal{E}, \mathcal{TS}) \mid \mathbf{X}_E \in \mathcal{T}_{\mathbf{m}_{E^+}} \mathcal{S} \text{ for all } E \in \mathcal{E}\}. \end{aligned}$$

2.3. Differential Geometry on the Simplex. In addition to the closed probability simplex

$$\Delta = \{\boldsymbol{\varphi} \in \mathbb{R}^L \mid \mathbf{1}^T \boldsymbol{\varphi} = 1, \boldsymbol{\varphi} \geq \mathbf{0}\},$$

we also require the open probability simplex

$$\tilde{\Delta} := \{\boldsymbol{\varphi} \in \mathbb{R}^L \mid \mathbf{1}^T \boldsymbol{\varphi} = 1, \boldsymbol{\varphi} > \mathbf{0}\}.$$

The tangent space $\mathcal{T}_{\boldsymbol{\varphi}} \tilde{\Delta}$ at any point $\boldsymbol{\varphi} \in \tilde{\Delta}$ is given by

$$\mathcal{T}_{\boldsymbol{\varphi}} \tilde{\Delta} = \{\mathbf{X} \in \mathbb{R}^L \mid \mathbf{1}^T \mathbf{X} = 0\}.$$

Using the Fisher-Rao metric, $\tilde{\Delta}$ can be equipped with a Riemannian manifold structure; see, e.g., [Åström et al., 2017](#), Sec. 2.1 for details. The geodesic distance

increases compared to the Euclidean distance close to the boundary. Given a point $\varphi \in \tilde{\Delta}$, the exponential map $\exp_\varphi: \mathcal{T}_\varphi \tilde{\Delta} \rightarrow \tilde{\Delta}$ is given by

$$(2.7) \quad \exp_\varphi(\mathbf{X}) = \frac{1}{2} \left(\varphi + \frac{\mathbf{X}_\varphi^2}{|\mathbf{X}_\varphi|^2} \right) + \frac{1}{2} \left(\varphi - \frac{\mathbf{X}_\varphi^2}{|\mathbf{X}_\varphi|^2} \right) \cos(|\mathbf{X}_\varphi|) + \frac{\sin(|\mathbf{X}_\varphi|)}{|\mathbf{X}_\varphi|} \mathbf{X}_\varphi \odot \sqrt{\varphi},$$

where $\mathbf{X}_\varphi = \mathbf{X}/\sqrt{\varphi}$ and $\odot, /, \sqrt{\cdot}$ are meant element-wise. Given a function $f: \mathbb{R}^L \rightarrow \mathbb{R}$ and a point $\varphi \in \tilde{\Delta}$, the Riemannian gradient $\text{grad}_{\tilde{\Delta}} f(\varphi)$ at φ can be computed using the Euclidean gradient $\nabla f(\varphi)$ by

$$(2.8) \quad \text{grad}_{\tilde{\Delta}} f(\varphi) = \nabla f(\varphi) \odot \varphi - (\varphi^T \nabla f(\varphi)) \varphi.$$

3. TWO TOTAL VARIATION REGULARIZERS

In this section, we discuss two regularizers \mathcal{R} for the model problem (1.1): the *assignment space total variation* (A-TV) and the *label space total variation* (L-TV). We recall from (1.1) the common framework is to find a piecewise constant assignment function $\varphi \in \mathcal{DG}(\mathcal{T}, \Delta)$ that minimizes

$$\underset{\varphi \in \mathcal{DG}(\mathcal{T}, \Delta)}{\text{Minimize}} \quad \sum_{T \in \mathcal{T}} |T| \sum_{\ell=1}^L s_\ell(\mathbf{n}_T) \varphi_{T,\ell} + \beta \mathcal{R}(\varphi).$$

In the absence of a regularizer ($\beta = 0$), the problem decouples and the minimum of $s_\ell(\mathbf{n}_T) \varphi_{T,\ell}$ is attained by the ℓ -th unit vector that corresponds to the label vector in $\{\mathbf{g}_1, \dots, \mathbf{g}_L\}$ that is closest to \mathbf{n}_T .

The purpose of the regularizer \mathcal{R} is to remove noise in the normal vector data and to enforce smoothness in the assignment function φ . Both regularizers are based on the total variation and thus they penalize the jumps of the assignment function φ between neighboring triangles.

3.1. Assignment Space Total Variation. In a straightforward adaptation of [Lellmann, Kappes, et al., 2009](#), we penalize the total variation of the assignment function φ . This leads to the *assignment space total variation*

$$(A-TV) \quad \underset{\varphi \in \mathcal{DG}(\mathcal{T}, \Delta)}{\text{Minimize}} \quad \sum_{T \in \mathcal{T}} |T| \sum_{\ell=1}^L s_\ell(\mathbf{n}_T) \varphi_{T,\ell} + \beta \text{TV}_\Delta(\varphi).$$

We equip the simplex Δ with $|\cdot|_1$, so that the total variation TV_Δ according to (2.1) becomes

$$(3.1) \quad \text{TV}_\Delta(\varphi) = \sum_{E \in \mathcal{E}} |E| |\varphi_{E_+} - \varphi_{E_-}|_1.$$

3.2. Label Space Total Variation. As an alternative to (A-TV), we propose a new regularizer that is based on the total variation in the label space \mathcal{S} . Since the value of the assignment function φ in the simplex Δ represents a mixture of labels, we now need to associate with φ a corresponding element $\mathbf{m}(\varphi)$ of the label space \mathcal{S} . Since the latter is a nonlinear space, a mixture of these labels is not simply a convex combination but rather a nonlinear weighted average, the

Riemannian center of mass (2.5). On the triangle T , this nonlinear mixture of the labels $\mathbf{g}_1, \dots, \mathbf{g}_L$ is given by

$$(3.2) \quad \mathbf{m}(\varphi)_T \in \arg \min_{\mathbf{m} \in \mathcal{S}} \sum_{\ell=1}^L \varphi_{T,\ell} d_{\mathcal{S}}(\mathbf{m}, \mathbf{g}_\ell)^2,$$

so that $\mathbf{m}(\varphi)$ is a piecewise constant function $\mathbf{m}(\varphi) \in \mathcal{DG}(\mathcal{T}, \mathcal{S})$. This leads to the *label space total variation* problem

$$(L\text{-TV}) \quad \text{Minimize}_{\varphi \in \mathcal{DG}(\mathcal{T}, \Delta)} \sum_{T \in \mathcal{T}} |T| \sum_{\ell=1}^L s_\ell(\mathbf{n}_T) \varphi_{T,\ell} + \beta \text{TV}_{\mathcal{S}}(\mathbf{m}(\varphi)).$$

In contrast to (3.1), the total variation term now considers the geodesic distances of neighboring Riemannian centers of mass,

$$(3.3) \quad \text{TV}_{\mathcal{S}}(\varphi) = \sum_{E \in \mathcal{E}} |E| d_{\mathcal{S}}(\mathbf{m}(\varphi)_{E_+}, \mathbf{m}(\varphi)_{E_-}).$$

Example 3.1 (Comparison of the regularizers). *To emphasize the difference of the newly proposed model (L-TV) compared to (A-TV), we compare the values of $\text{TV}_{\Delta}(\varphi)$ and $\text{TV}_{\mathcal{S}}(\mathbf{m}(\varphi))$ for two different assignments φ and $\tilde{\varphi}$. The situation is illustrated in Figure 3.1. Normalizing the edges where jumps occur to length one, we evaluate*

$$(3.4) \quad 2 = \text{TV}_{\Delta}(\varphi) < \text{TV}_{\Delta}(\tilde{\varphi}) = 4, \quad \text{TV}_{\mathcal{S}}(\mathbf{m}(\varphi)) = \text{TV}_{\mathcal{S}}(\mathbf{m}(\tilde{\varphi})) = \frac{\pi}{2}.$$

This clarifies that the assignment of an intermediate label between two assigned labels incurs an additional penalty in the assignment space total variation model (A-TV) but not in the (L-TV) model. This hints at the fact later confirmed by our numerical experiments that the (A-TV) model tends to “skip” labels to reduce the regularization penalty.

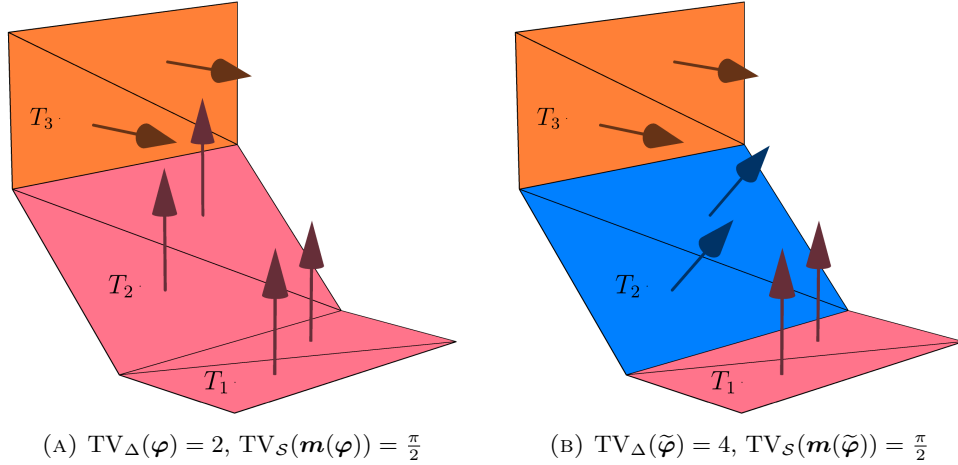


FIGURE 3.1. Visualization of the assignments $\varphi, \tilde{\varphi}$ as described in Example 3.1.

4. NUMERICAL ALGORITHMS

In this section, we present numerical methods for both models. The simpler assignment space total variation problem (A-TV) can actually be rewritten as a linear program with $(|\mathcal{T}| + |\mathcal{E}|) \cdot L$ variables, $2L \cdot |\mathcal{E}|$ inequality constraints and $|\mathcal{T}|$ equality constraints. In our largest problem instance (Section 5.2), this amounts to more than 1.4 million variables. While problems of this size, particularly with sparse constraint matrices, can be handled by state-of-the-art solvers, in this study we use the Chambolle-Pock algorithm [Chambolle, Pock, 2011](#); [Pock et al., 2009](#). This leads to very simple and parallelizable update steps.

The Chambolle-Pock method cannot be directly applied to the label space assignment problem (L-TV), because the Riemannian center of mass $\mathbf{m}(\varphi)$ does not depend linearly on the assignment φ . We therefore use an alternating direction method of multipliers (ADMM) [Boyd et al., 2010](#), whose individual steps are also parallelizable and mostly simple.

4.1. Chambolle-Pock Algorithm for Assignment Space Total Variation.

For problem (A-TV), we use the Chambolle-Pock algorithm [Pock et al., 2009](#), similarly as in [Chambolle, Pock, 2011](#), Section 6.3.4. To set up the algorithm, we introduce the jump operator K

$$(4.1) \quad K: \mathcal{DG}(\mathcal{T}, \Delta) \rightarrow \mathcal{DG}(\mathcal{E}, \mathbb{R}^L), \quad (K\varphi)_E := \beta(\varphi_{E_+} - \varphi_{E_-}).$$

The algorithm can be written as shown in [Algorithm 1](#), where K^* denotes the Hilbert-space adjoint of K w.r.t. the L^2 -inner products on $\mathcal{DG}(\mathcal{T}, \mathbb{R}^L)$ and $\mathcal{DG}(\mathcal{E}, \mathbb{R}^L)$. These inner products are represented by diagonal matrices with the triangle areas or edge lengths on the diagonal, respectively.

Algorithm 1 Chambolle-Pock algorithm applied to the assignment space total variation problem (A-TV).

Input: similarity measure $\mathbf{s} \in \mathcal{DG}(\mathcal{T}, \mathbb{R}^L)$

Input: step sizes $\tau > 0$, $\sigma > 0$, extrapolation parameter $\theta \in [0, 1]$

Input: $\varphi^{(0)} \in \mathcal{DG}(\mathcal{T}, \Delta)$, $\mathbf{v}^{(0)} \in \mathcal{DG}(\mathcal{E}, \mathbb{R}^L)$

Output: approximate solution of (A-TV)

- 1: Set $\bar{\varphi}^{(0)} \leftarrow \varphi^{(0)}$
 - 2: **while** not converged **do**
 - 3: Set $\mathbf{v}_E^{(k+1)} \leftarrow \text{clip}(\mathbf{v}_E^{(k)} + \sigma[K\bar{\varphi}^{(k)}]_E, -1, 1)$ for all edges E
 - 4: Set $\varphi_T^{(k+1)} \leftarrow \text{proj}_\Delta(\varphi_T^{(k)} - \tau[K^*\mathbf{v}^{(k+1)} - \tau\mathbf{s}]_T)$ for all triangles T
 - 5: Set $\bar{\varphi}^{(k+1)} \leftarrow \varphi^{(k+1)} + \theta(\varphi^{(k+1)} - \varphi^{(k)})$
 - 6: $k \leftarrow k + 1$
 - 7: **end while**
-

Here, the clipping operator $\text{clip}(\cdot, -1, 1): \mathbb{R}^L \rightarrow [-1, 1]^L$ projects each component to the interval $[-1, 1]$. Further, the simplex projection proj_Δ in [Line 4](#) can be efficiently computed using [Algorithm 1](#) in [Wang, Carreira-Perpiñán, 2013](#).

4.2. ADMM for Label Space Total Variation. [Algorithm 1](#) cannot be transferred easily to the label space assignment problem (L-TV), because the Riemannian center of mass $\mathbf{m}(\varphi)$ does not depend linearly on the assignment φ . A method

applicable to (L-TV) is the alternating direction method of multipliers (ADMM); see [Boyd et al., 2010](#); [Goldstein, Osher, 2009](#).

We now derive the specific form of that algorithm. In addition to the assignment variable $\varphi \in \mathcal{DG}(\mathcal{T}, \Delta)$, we introduce three auxiliary variables \mathbf{m} , \mathbf{Y} , and \mathbf{X} . As is customary in ADMM, the purpose of these variables is to allow problem (L-TV) to be split into simpler subproblems. Each of the auxiliary variables is coupled to the remaining variables through a constraint that is enforced by a penalty term in the augmented Lagrangian function.

The first auxiliary variable $\mathbf{m} \in \mathcal{DG}(\mathcal{T}, \mathcal{S})$ represents the Riemannian center of mass of the labels, weighted according to the assignment function φ per triangle. We introduce the necessary optimality condition (2.6) of the weighted Riemannian center of mass problem as the corresponding constraint. In fact, we replace the nonlinear terms $\log_{\mathbf{m}}(\mathbf{g}_\ell)$ in (2.6), triangle by triangle, by the auxiliary variable $\mathbf{Y} \in \mathcal{DG}(\mathcal{T}, \mathcal{TS})$. This leaves us with the constraint (2.6) in the form $\sum_{\ell=1}^L \varphi_{T,\ell} \mathbf{Y}_{T,\ell} = \mathbf{0}$ as well as $\mathbf{Y}_{T,\ell} = \log_{\mathbf{m}_T}(\mathbf{g}_\ell)$. For numerical stability, we represent the latter in the form $\mathbf{g}_\ell = \exp_{\mathbf{m}_T} \mathbf{Y}_{T,\ell}$.

Finally, to handle the non-smoothness in the total variation (3.3), we introduce the third auxiliary variable $\mathbf{X} \in \mathcal{DG}(\mathcal{E}, \mathcal{TS})$ coupled by the constraint $\mathbf{X}_E = \log_{\mathbf{m}_{E_+}}(\mathbf{m}_{E_-})$. We thus arrive at

$$(4.2) \quad \begin{aligned} & \underset{\varphi, \mathbf{m}, \mathbf{Y}, \mathbf{X}}{\text{Minimize}} && \sum_{T \in \mathcal{T}} |T| \varphi_T^T \mathbf{s}_T + \beta \sum_{E \in \mathcal{E}} |E| |\mathbf{X}_E|_2 \\ & \text{subject to} && \begin{cases} \mathbf{0} = \sum_{\ell=1}^L \varphi_{T,\ell} \mathbf{Y}_{T,\ell} \in \mathcal{T}_{\mathbf{m}_T} \mathcal{S} & \text{for all } T \in \mathcal{T}, \\ \mathbf{g}_\ell = \exp_{\mathbf{m}_T} \mathbf{Y}_{T,\ell} \in \mathcal{S} \subseteq \mathbb{R}^3 & \text{for all } T \in \mathcal{T}, \ell = 1, \dots, L, \\ \mathbf{X}_E = \log_{\mathbf{m}_{E_+}}(\mathbf{m}_{E_-}) \in \mathcal{T}_{\mathbf{m}_{E_+}} \mathcal{S} & \text{for all } E \in \mathcal{E}. \end{cases} \end{aligned}$$

Notice that (4.2) is not strictly equivalent to (L-TV), because we use a necessary, but not sufficient, optimality condition to substitute the Riemannian center of mass \mathbf{m} . In practice, we did not observe any difficulties stemming from this discrepancy.

We associate with problem (4.2) the following augmented Lagrangian

$$(4.3) \quad \begin{aligned} & \mathcal{L}_\rho(\varphi, \mathbf{m}, \mathbf{Y}, \mathbf{X}, \boldsymbol{\lambda}, \boldsymbol{\mu}, \boldsymbol{\nu}) \\ & = \sum_{T \in \mathcal{T}} |T| \varphi_T^T \mathbf{s}_T + \beta \sum_{E \in \mathcal{E}} |E| |\mathbf{X}_E|_2 + \frac{\rho}{2} \sum_{T \in \mathcal{T}} |T| \left| \sum_{\ell=1}^L \varphi_{T,\ell} \mathbf{Y}_{T,\ell} + \boldsymbol{\lambda}_T \right|_2^2 \\ & \quad + \frac{\rho}{2} \sum_{T \in \mathcal{T}} |T| \sum_{\ell=1}^L \left| \exp_{\mathbf{m}_T}(\mathbf{Y}_{T,\ell}) - \mathbf{g}_\ell + \boldsymbol{\mu}_{T,\ell} \right|_2^2 \\ & \quad + \frac{\rho}{2} \sum_{E \in \mathcal{E}} |E| \left| \log_{\mathbf{m}_{E_+}}(\mathbf{m}_{E_-}) - \mathbf{X}_E + \boldsymbol{\nu}_E \right|_2^2. \end{aligned}$$

The quantities $\boldsymbol{\lambda} \in \mathcal{DG}(\mathcal{T}, \mathbb{R}^3)$, $\boldsymbol{\mu} \in \mathcal{DG}(\mathcal{T}, \mathbb{R}^{L \times 3})$, as well as $\boldsymbol{\nu} \in \mathcal{DG}(\mathcal{E}, \mathbb{R}^3)$ represent the (rescaled) Lagrange multipliers associated with the constraints in (4.2). The values of \mathbf{X} and \mathbf{Y} need to be constrained to belong to the respective tangent spaces of \mathcal{S} . Depending on \mathbf{m} , the same applies to $\boldsymbol{\lambda}$ and $\boldsymbol{\nu}$. This is addressed in for each variable separately in the following subsections.

In each iteration of ADMM, we subsequently minimize the augmented Lagrangian (4.3) with respect to one of the primal variables while fixing the others. We choose \mathbf{Y} , \mathbf{X} , $\boldsymbol{\varphi}$, \mathbf{m} as the order of updates in order to best exploit the problem structure. Specifically, the \mathbf{Y} and \mathbf{X} problems turn out to be independent of each other, and likewise the $\boldsymbol{\varphi}$ and \mathbf{m} problems are independent of each other as well.

We now address each of the four primal problems individually. The index $\cdot^{(k)}$ denotes the iteration number. The overall ADMM algorithm is described in Section 4.2.5.

4.2.1. *The \mathbf{Y} -Subproblem.* The minimization of (4.3) with respect to \mathbf{Y} decouples into independent smooth problems, one on each triangle T . Omitting the terms that do not depend on \mathbf{Y} as well as the factor $\frac{\rho}{2}|T|$ common to all remaining terms, we obtain

$$(4.4) \quad \underset{\mathbf{Y}_{T \in (\mathcal{T}_{\mathbf{m}_T \mathcal{S}})^L}}{\text{Minimize}} \quad \left| \sum_{\ell=1}^L \boldsymbol{\varphi}_{T,\ell}^{(k)} \mathbf{Y}_{T,\ell} + \boldsymbol{\lambda}_T^{(k)} \right|_2^2 + \sum_{\ell=1}^L \left| \exp_{\mathbf{m}_T^{(k)}}(\mathbf{Y}_{T,\ell}) - \mathbf{g}_\ell + \boldsymbol{\mu}_{T,\ell}^{(k)} \right|_2^2.$$

We solve these problems simultaneously by applying a (Euclidean) gradient descent scheme with an Armijo backtracking strategy in the space $\mathcal{DG}(\mathcal{T}, \mathcal{TS}, \mathbf{m})$. In fact, we check a stopping criterion per triangle and drop the converged triangles from subsequent gradient steps. As stopping criterion we use $|\nabla_{\mathbf{Y}_T} \mathcal{L}_\rho| \leq \max\{10^{-8}, 10^{-0.0025k}\}$, dependent on the iteration number k of the outer ADMM loop. The overall solution of the \mathbf{Y} -subproblem obtained in this way is denoted by $\mathbf{Y}_T^{(k+1)}$.

4.2.2. *The \mathbf{X} -Subproblem.* The minimization of (4.3) with respect to \mathbf{X} also decouples into independent problems, one on each edge E . Omitting the terms that do not depend on \mathbf{X} as well as the factor $|E|$ common to all remaining terms, we obtain

$$(4.5) \quad \underset{\mathbf{X}_E \in \mathcal{T}_{\mathbf{m}_{E_+}^{(k)}} \mathcal{S}}{\text{Minimize}} \quad \beta |\mathbf{X}_E|_2 + \frac{\rho}{2} \left| \log_{\mathbf{m}_{E_+}^{(k)}}(\mathbf{m}_{E_-}^{(k)}) - \mathbf{X}_E + \boldsymbol{\nu}_E^{(k)} \right|_2^2.$$

This problem is well known to have a closed-form solution in terms of a vector-valued soft-thresholding operation; see for instance Goldstein, Osher, 2009. We obtain

$$(4.6) \quad \mathbf{X}_E^{(k+1)} = \left(1 - \frac{\beta/\rho}{\max\{\beta/\rho, |\log_{\mathbf{m}_{E_+}^{(k)}}(\mathbf{m}_{E_-}^{(k)}) + \boldsymbol{\nu}_E^{(k)}|_2\}} \right) \left(\log_{\mathbf{m}_{E_+}^{(k)}}(\mathbf{m}_{E_-}^{(k)}) + \boldsymbol{\nu}_E^{(k)} \right).$$

The result $\mathbf{X}_E^{(k+1)}$ is naturally an element of the tangent space $\mathcal{T}_{\mathbf{m}_{E_+} \mathcal{S}}$, because both $\log_{\mathbf{m}_{E_+}^{(k)}}(\mathbf{m}_{E_-}^{(k)})$ and $\boldsymbol{\nu}_E^{(k)}$ are.

4.2.3. *The $\boldsymbol{\varphi}$ -Subproblem.* Concerning $\boldsymbol{\varphi}$, the minimization of (4.3) decouples into independent quadratic programming problems (QPs), one on each triangle T . Omitting the terms that do not depend on $\boldsymbol{\varphi}$ as well as the factor $|T|$ common to all remaining terms, we obtain

$$(4.7) \quad \underset{\boldsymbol{\varphi}_T \in \Delta}{\text{Minimize}} \quad \boldsymbol{\varphi}_T^T \mathbf{s}_T + \frac{\rho}{2} \left| \sum_{\ell=1}^L \boldsymbol{\varphi}_{T,\ell} \mathbf{Y}_{T,\ell}^{(k+1)} + \boldsymbol{\lambda}_T^{(k)} \right|_2^2.$$

This is a standard convex QP with constraints $\boldsymbol{\varphi}^T \mathbf{1} = 0$ and $\boldsymbol{\varphi} \geq \mathbf{0}$. We initially solved these problems using the QP solver OSQP from [Stellato et al., 2020](#). However, we found that a specialized solver exploiting the geometry of the probability simplex can be more efficient, particularly in light of the fact that we need to solve one problem of type (4.7) for each triangle and each iteration of the ADMM algorithm, which may easily amount to millions of QPs solved.

We proceed in a two-stage procedure to solve (4.7). In the first stage, we apply a Riemannian gradient descent scheme with an Armijo backtracking strategy on the open probability simplex $\tilde{\Delta}$. This makes use of the exponential map (2.7) and of the Riemannian gradient (2.8) of the objective in (4.7). The gradient scheme stops when the iterates approach the boundary, i. e., when a component φ_ℓ becomes small, or when the norm of the Riemannian gradient falls below a threshold.

The approximate solution obtained in this way serves to determine the inactive and active inequalities, i. e., the subsets $\mathcal{I}, \mathcal{A} \subseteq \{1, \dots, L\}$, where $\varphi_{T,\ell} = 0$ on the latter. With the active set \mathcal{A} and its complement \mathcal{I} at hand, the KKT system for (4.7) becomes a linear system of equations,

$$(4.8) \quad \begin{aligned} \mathbf{0} &= \rho \mathbf{Y}_T \mathbf{Y}_T^T \boldsymbol{\varphi}_T + \rho \mathbf{Y}_T \boldsymbol{\lambda}_T + \mathbf{s}_T - \boldsymbol{\alpha}_T - \gamma_T \mathbf{1}, \\ 1 &= \mathbf{1}^T \boldsymbol{\varphi}_T, \\ 0 &= \varphi_{T,\ell} \quad \text{for } \ell \in \mathcal{A}, \\ 0 &= \alpha_{T,\ell} \quad \text{for } \ell \in \mathcal{I}. \end{aligned}$$

The variables $\boldsymbol{\alpha}_T \in \mathbb{R}^L$ and $\gamma_T \in \mathbb{R}$ are the Lagrange multipliers associated with the constraints $\varphi_{T,\ell} = 0$ and $\mathbf{1}^T \boldsymbol{\varphi}_T = 1$, respectively. If a solution $(\boldsymbol{\varphi}_T, \boldsymbol{\alpha}_T, \gamma_T)$ to the KKT system (4.8) exists and fulfills $\boldsymbol{\varphi}_T \geq \mathbf{0}$ (primal feasibility) and $\boldsymbol{\alpha}_T \geq \mathbf{0}$ (dual feasibility), then $\boldsymbol{\varphi}_T$ is in fact a solution to the original problem (4.7). We then assign it to $\boldsymbol{\varphi}_T^{(k+1)}$. Otherwise, the estimate of the active set was incorrect and we use the result of the Riemannian gradient descent stage for $\boldsymbol{\varphi}_T^{(k+1)}$ as a fallback. The entire procedure is shown in [Algorithm 2](#).

4.2.4. *The \mathbf{m} -Subproblem.* It remains to discuss the update for the variable \mathbf{m} representing the Riemannian center of mass (3.2). Omitting the terms that do not depend on \mathbf{m} as well as the factor $\frac{\rho}{2}$ common to all remaining terms, we obtain

$$\begin{aligned} \text{Minimize}_{\mathbf{m} \in \mathcal{DG}(\mathcal{T}, \mathcal{S})} \quad & \sum_{T \in \mathcal{T}} |T| \sum_{\ell=1}^L \left| \exp_{\mathbf{m}_T}(\mathbf{Y}_{T,\ell}^{(k+1)}) - \mathbf{g}_\ell + \boldsymbol{\mu}_{T,\ell}^{(k)} \right|_2^2 \\ & + \sum_{E \in \mathcal{E}} |E| \left| \log_{\mathbf{m}_{E_+}}(\mathbf{m}_{E_-}) - \mathbf{X}_E^{(k+1)} + \boldsymbol{\nu}_E^{(k)} \right|_2^2. \end{aligned}$$

Note, however, that a change of the variable \mathbf{m} always requires a simultaneous update of the tangent vectors $\mathbf{Y}, \mathbf{X}, \boldsymbol{\lambda}, \boldsymbol{\nu}$ to the tangent space of \mathcal{S} at \mathbf{m} . We therefore consider these variables to be dependent on \mathbf{m} and replace them by their parallelly transported counterparts, leading to

$$(4.9) \quad \begin{aligned} \text{Minimize}_{\mathbf{m} \in \mathcal{DG}(\mathcal{T}, \mathcal{S})} \quad & \sum_{T \in \mathcal{T}} |T| \sum_{\ell=1}^L \left| \exp_{\mathbf{m}_T}(\mathbf{P}_{\mathbf{m}_T \leftarrow \mathbf{m}_T^{(k)}}(\mathbf{Y}_{T,\ell}^{(k+1)})) - \mathbf{g}_\ell + \boldsymbol{\mu}_{T,\ell}^{(k)} \right|_2^2 \\ & + \sum_{E \in \mathcal{E}} |E| \left| \log_{\mathbf{m}_{E_+}}(\mathbf{m}_{E_-}) + \mathbf{P}_{\mathbf{m}_T \leftarrow \mathbf{m}_{E_+}^{(k)}}(-\mathbf{X}_E^{(k+1)} + \boldsymbol{\nu}_E^{(k)}) \right|_2^2. \end{aligned}$$

Algorithm 2 Solution of the simplex-constrained QP (4.7), the φ -subproblem

Input: $\mathbf{s}_T \in \mathbb{R}^L$, $\mathbf{Y}_T \in (\mathcal{T}_{m_T} \mathcal{S})^L$, $\boldsymbol{\lambda}_T \in \mathcal{T}_{m_T} \mathcal{S}$,

Input: $\varphi_T^{(0)} \in \Delta$, $\varepsilon > 0$, $\text{TOL}_1, \text{TOL}_2, \text{TOL}_3 > 0$

Output: approximate solution of (4.7)

```

1: Set  $j \leftarrow 0$ 
2: Set  $\varphi_T^{(0)} \leftarrow \frac{1}{1+\varepsilon L} (\varphi_T^{(0)} + \varepsilon \mathbf{1})$  // recentralize  $\varphi_T^{(0)}$  to the open simplex  $\tilde{\Delta}$ 
3: while  $|\text{grad}_{\tilde{\Delta}} f_T(\varphi_T^{(j)})| > \text{TOL}_1$  and  $\min\{\varphi_{T,\ell}^{(j)} \mid 1 \leq \ell \leq L\} > \text{TOL}_2$  do
4:   Set  $\varphi_T^{(j+1)} \leftarrow \exp_{\varphi_T^{(j)}}(-\boldsymbol{\alpha}_T^{(j+1)} \text{grad}_{\tilde{\Delta}} f_T(\varphi_T^{(j)}))$ 
5:   Set  $j \leftarrow j + 1$ 
6: end while // end of stage 1
7:  $\mathcal{A} = \{1 \leq \ell \leq L \mid \varphi_{T,\ell}^{(j)} > \text{TOL}_3\}$ 
8: Solve the KKT system (4.8) for  $(\varphi_T, \boldsymbol{\alpha}_T, \gamma_T)$ 
9: if  $\boldsymbol{\alpha}_T, \varphi_T \geq \mathbf{0}$  then
10:  return  $\varphi_T$  // solution of (4.7)
11: else
12:  return  $\varphi_T^{(j)}$  // return the result of stage 1 as fallback
13: end if

```

We solve this problem only approximately, using a Riemannian gradient descent scheme with an Armijo backtracking strategy in the space $\mathcal{DG}(\mathcal{T}, \mathcal{S})$. Notice that this problem does not decompose over mesh entities since it contains both a sum over triangles and a sum over edges. The iteration is stopped when a maximum of 20 gradient steps is reached, or when the condition $|\nabla_{\mathbf{m}} \mathcal{L}_\rho| \leq \max\{10^{-8}, 10^{-0.0025k}\}$ is fulfilled. The overall solution of the \mathbf{m} -subproblem obtained in this way is denoted by $\mathbf{m}^{(k+1)}$. When the gradient descent scheme terminates, we leave the tangent vectors $\mathbf{Y}^{(k+1)}$, $\mathbf{X}^{(k+1)}$, $\boldsymbol{\lambda}^{(k)}$, $\boldsymbol{\nu}^{(k)}$ in their respective tangent spaces pertaining to the new iterate $\mathbf{m}^{(k+1)}$.

4.2.5. *Overall ADMM Scheme.* The overall ADMM scheme for the solution of the label space total variation problem (L-TV) in the form of (4.2) is summarized in Algorithm 3. As was mentioned before, due to the independence of the \mathbf{Y} and \mathbf{X} problems, as well as the φ and \mathbf{m} problems, Lines 2 and 3 as well as Lines 4 and 5 can be executed in parallel.

5. NUMERICAL EXAMPLES

In this section, we compare the solutions of the proposed segmentation problems (A-TV) and (L-TV) for a number of label sets and two different surfaces. For each example, we proceed as follows. We begin with a mesh Γ and add Gaussian noise to the vertex positions. The vertex-dependent variance is chosen as $\sigma^2 = 0.04e^2$ and it scales with the average length e of the edges adjacent to the respective vertex. We then solve (A-TV) using Algorithm 1 and (L-TV) using Algorithm 3.

Since the two variants of total variation penalty are not directly comparable by value, we choose the penalty parameter β independently for each model and example. In each case, we experimentally determine the optimal value β^* in the following way. We solve the assignment problem with $\beta = 0$ for the mesh without noise, which simply amounts to finding the index where $\mathbf{s}_{T,\ell}$ is minimal on each

Algorithm 3 ADMM for the label space total variation problem (4.2).

Input: labels $\mathbf{g}_1, \dots, \mathbf{g}_L \in \mathcal{S}$, similarity measure $\mathbf{s} \in \mathcal{DG}(\mathcal{T}, \mathbb{R}^L)$

Input: TV penalty parameter $\beta > 0$, augmentation parameter $\rho > 0$

Input: $\varphi^{(0)} \in \mathcal{DG}(\mathcal{T}, \Delta)$, $\mathbf{m}^{(0)} \in \mathcal{DG}(\mathcal{T}, \mathcal{S})$,

Input: $\mathbf{Y}^{(0)} \in \mathcal{DG}(\mathcal{T}, \mathcal{TS}, \mathbf{m}^{(0)})^L$, $\mathbf{X}^{(0)} \in \mathcal{DG}(\mathcal{E}, \mathcal{TS}, \mathbf{m}^{(0)})$

Output: approximate solution of (4.2)

1: **while** not converged **do**

2: Use a gradient descent scheme to find an approximate minimizer $\mathbf{Y}^{(k+1)}$ of (4.4); see Section 4.2.1

3: Set $\mathbf{X}^{(k+1)}$ using the soft-thresholding operation (4.6); see Section 4.2.2

4: Set $\varphi^{(k+1)}$ to the solution of (4.7), using Algorithm 2; see Section 4.2.3

5: Use a Riemannian gradient descent scheme to find an approximate minimizer $\mathbf{m}^{(k+1)}$ of (4.9); see Section 4.2.4

 Update the Lagrange multipliers:

6: $\lambda_T^{(k+1)} \leftarrow \lambda_T^{(k)} + \sum_{\ell=1}^L \varphi_{T,\ell}^{(k+1)} \mathbf{Y}_{T,\ell}^{(k+1)}$ for all $T \in \mathcal{T}$

7: $\mu_{T,\ell}^{(k+1)} \leftarrow \mu_{T,\ell}^{(k)} + \exp_{\mathbf{m}_T^{(k+1)}}(\mathbf{Y}_{T,\ell}^{(k+1)}) - \mathbf{g}_\ell$ for all $T \in \mathcal{T}$ and $\ell = 1, \dots, L$

8: $\nu_E^{(k+1)} \leftarrow \nu_E^{(k)} + \log_{\mathbf{m}_{E_-}^{(k+1)}}(\mathbf{m}_{E_+}^{(k+1)}) - \mathbf{X}_E^{(k+1)}$ for all $E \in \mathcal{E}$

9: **end while**

triangle T . We then pick β^* as the value of β that gives the best result in terms of the minimal number of wrongly labeled triangles, weighted by triangle area. We also show the results for larger and smaller values of β to show the sensitivity to variations of this parameter.

The assignment function φ takes values in the simplex Δ but not necessarily equal to a vertex. That is, some triangles will be ambiguously labeled, which needs to be resolved both for the purpose of visualization as well as for the procedure to select the optimal penalty parameter β^* . To this end, we simply choose the label with the highest assignment value per triangle in case of the assignment space total variation problem (A-TV). For the label space total variation problem (L-TV), we choose the label \mathbf{g}_ℓ with the smallest geodesic distance to the assigned normal $\mathbf{m}(\varphi)_T$. We found this to be a more natural choice in view of the mapping $\varphi_T \mapsto \mathbf{m}(\varphi_T)$ not being injective so that several assignments φ_T yield the same Riemannian center of mass $\mathbf{m}(\varphi_T)$.

The code for the numerical experiments is written in PYTHON using the FENICS finite element library version 2019.1 Alnæs et al., 2015. It was run in parallel using 15 cores on an Intel Quad Xeon CPU@2.6 GHz compute server. The parallelization is based on the built-in MPI support provided by FENICS, which essentially addresses the subproblems in Algorithms 1 and 3 by way of domain decomposition. We do not exploit the possible parallel execution of the update steps of \mathbf{Y} and \mathbf{X} and, respectively, φ and \mathbf{m} , as mentioned in Section 4.2.5.

As expected, the more complex label space assignment TV model (L-TV) requires a higher computational effort than the assignment TV model (A-TV). In general, the computation time roughly depends on the size of the mesh, the number of labels L and the TV regularization parameter β . Table 5.1 shows the approximate run time for the experiments presented in the subsequent sections, each for the

	(A-TV)	(L-TV)
unit sphere mesh	50 s	1840 s
fandisk mesh, nonuniform labels	70 s	2790 s
fandisk mesh, uniform labels	370 s	4760 s

TABLE 5.1. Approximate run times for the different algorithms on an Intel Quad Xeon CPU.

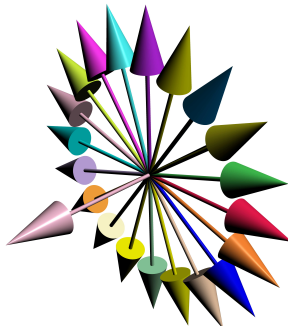


FIGURE 5.1. Visualization of the label set (5.1) for the sphere mesh example (Section 5.1).

respective optimal value of β^* . We observe that the (L-TV) model requires considerable more CPU time compared to the (A-TV) model. The main computational effort in the label space TV model is due to the \mathbf{m} -subproblem (Section 4.2.4), which is a coupled nonlinear problem over the entire mesh. Although this is beyond the scope of the present paper, future work should address opportunities for acceleration of this step.

5.1. Unit Sphere Mesh. The first mesh we consider is a discretization of the unit sphere $\mathcal{S} \subseteq \mathbb{R}^3$ into 4554 triangles. We choose the labels to form an equidistant partition around the equator, plus the poles, namely

$$(5.1) \quad \mathbf{g}_\ell := \begin{pmatrix} \sin\left(\ell \cdot \frac{2\pi}{20}\right) \\ \cos\left(\ell \cdot \frac{2\pi}{20}\right) \\ 0 \end{pmatrix} \text{ for } \ell = 1, \dots, 20, \quad \mathbf{g}_{21} = \begin{pmatrix} 0 \\ 0 \\ 1 \end{pmatrix} \text{ and } \mathbf{g}_{22} = -\mathbf{g}_{21}.$$

The labels are visualized in Figure 5.1.

Figure 5.2 shows the resulting assignments for this setup. For each of the two models, we choose $\beta \in \{1/4, 1, 4\} \cdot \beta^*$, where β^* is the optimal parameter choice for the respective model.

For the optimal parameter $\beta_{\text{A-TV}}^*$, the solution of the (A-TV) model uses 21 out of the available 22 labels. However, 6 of the labels are used only on a very small number of triangles and are not visible in Figure 5.2. Overall, 69.5% of all triangles are correctly labeled. By contrast, the new (L-TV) uses all 22 labels evenly and achieves a correctness of 86.7%.

The sphere mesh together with our choice of labels illustrates that the label space total variation model (L-TV) incurs no additional regularization penalties

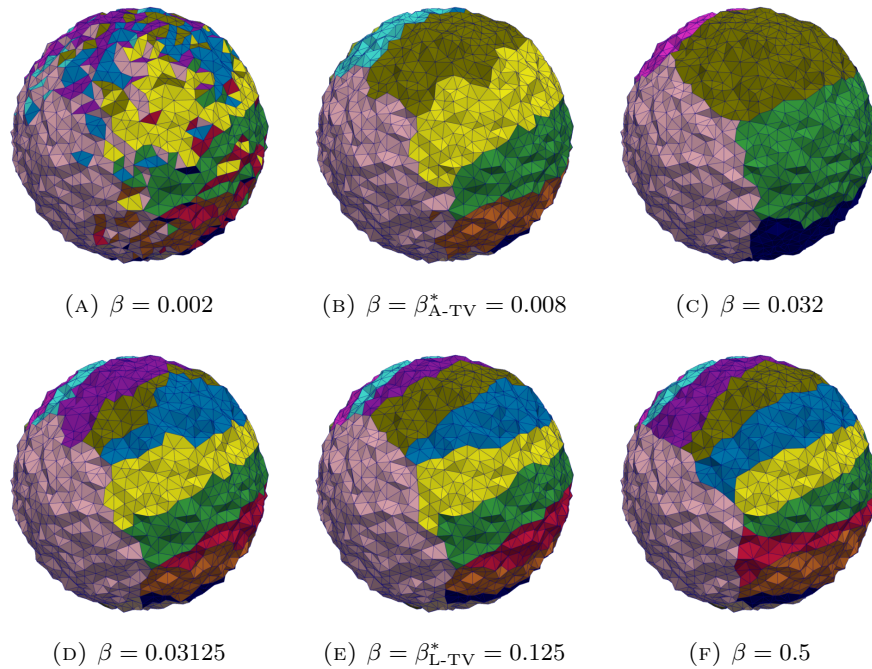


FIGURE 5.2. Assignments for the noisy sphere mesh with different values of β and the label set depicted in Figure 5.1. Triangles are colored according to their assigned label. One of the poles is shown in light pink. Figures 5.2a to 5.2c show the results using (A-TV), while Figures 5.2d to 5.2f show the results using the new (L-TV) model.

for “in-between labels”; see also Example 3.1 and the discussion there. Therefore, it is able to use all available labels.

A second benefit of the new model is its robustness with respect to the choice of the regularization parameter. In case of too small a regularization parameter (Figure 5.2a), we see that (A-TV) fails to produce segment the mesh in a meaningful way, in contrast to (L-TV). For too large a regularization parameter (Figure 5.2c), the assignment space total variation model (A-TV) does produce meaningful segments, but only uses a subset of the of the available labels, while the label space total variation model (L-TV) still uses all 22.

5.2. Fandisk Mesh. Next, we consider the fandisk mesh from Hoppe et al., 1994, which is available at the Wolfram Data Respository Shedelbower, 2022. As above, we added Gaussian noise to the vertex positions. For this example, we consider two different label sets. The first label set has 29 labels and they are chosen to represent the normals occurring on the round parts of the fandisk mesh well. The aim is to allow for a finer segmentation of the mesh on said parts.

By contrast, the second label set consists of 50 labels that are distributed uniformly on the sphere. We obtain this label set using a Fibonacci lattice; see González, 2009. The labels sets are visualized in Figure 5.3.

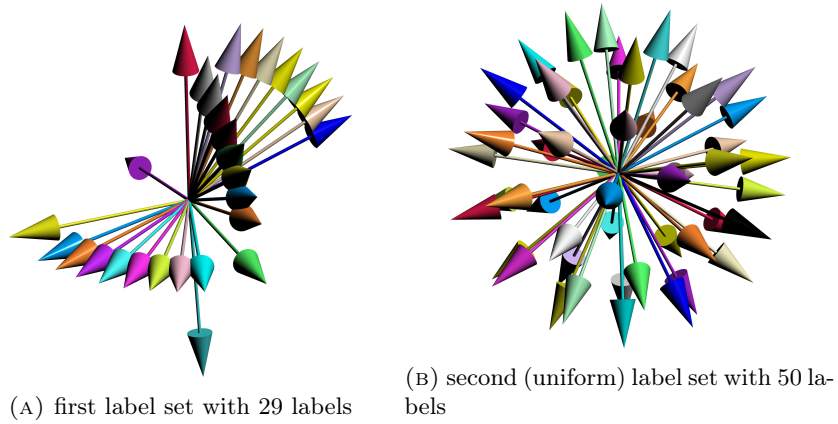


FIGURE 5.3. Visualization of the two label sets for the fandisk mesh example (Section 5.2).

The results for the first label set are shown in Figure 5.4. For each of the two models, we choose $\beta \in \{1/2, 1, 2\} \cdot \beta^*$, where β^* is the optimal parameter choice for the respective model. For the optimal parameter $\beta_{\text{A-TV}}^*$, the solution of the (A-TV)

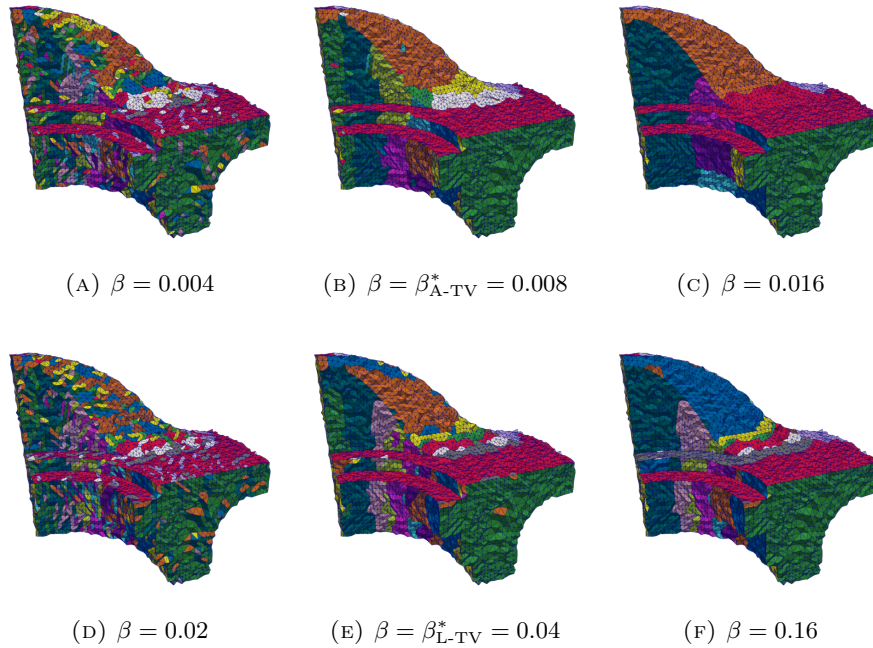


FIGURE 5.4. Assignments for the noisy fandisk mesh with the first label set of 29 labels (Figure 5.3a) and different values of β . Triangles are colored according to their assigned label. Figures 5.4a to 5.4c show the results using (A-TV), while Figures 5.4d to 5.4f show the results using (L-TV).

model uses 26 out of the available 29 labels and correctly labels 89.6% of the triangles. By contrast, the new (L-TV) uses 27 labels and achieves a correctness of 91.4%. We observe that the (L-TV) is able to assign a more detailed segmentation of the round parts in the front both for the optimal parameter β_{L-TV}^* and also for $2\beta_{L-TV}^*$. This shows that for this setup, the (L-TV) is again more robust against choosing a regularization parameter β that is too large. Both models fail to produce a meaningful segmentation when the regularization parameter is $\beta^*/2$.

The results for the second label set are shown in Figure 5.5. In this case, the

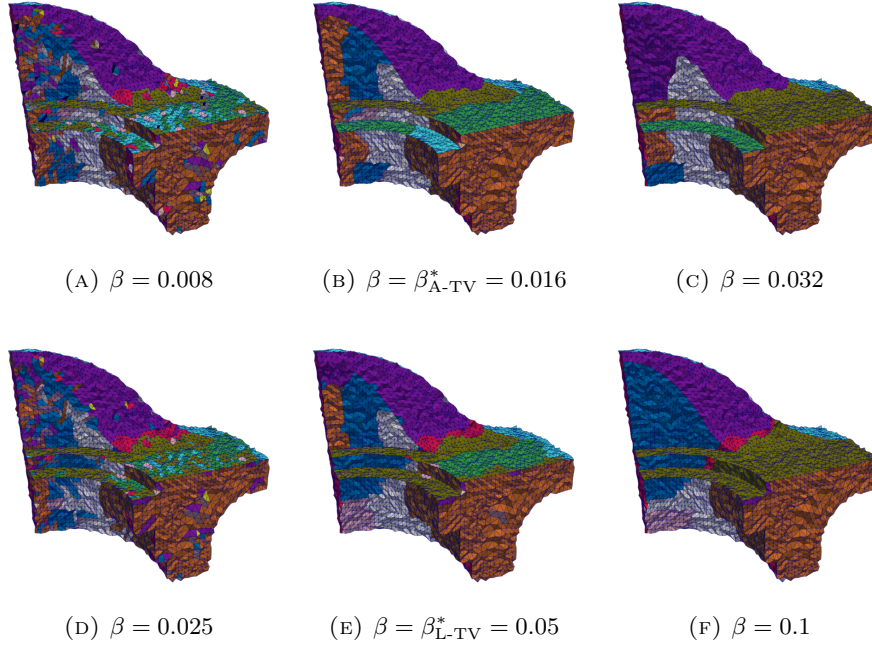


FIGURE 5.5. Assignments for the noisy fan disk mesh with the second label set of 50 uniformly distributed labels (Figure 5.3b) with different values of β . Triangles are colored according to their assigned label. Figures 5.5a to 5.5c show the results using (A-TV), while Figures 5.5d to 5.5f show the results using (L-TV).

(A-TV) model uses 26 of the available 50 labels and correctly labels 86.8% of the mesh, while the (L-TV) model uses 37 labels and correctly labels 85.2% of the mesh. We see that the latter is having difficulties in removing the noise near the sharp boundaries between labels, even for high values of the regularization parameter β . However, the label space TV model (L-TV) also is able to more precisely recover the round parts of the original mesh and remove the noise.

6. CONCLUSION

In this paper, we have compared two variational models for the segmentation of triangulated surfaces. The classical assignment space total variation model (A-TV) penalizes the total variation of the assignment function directly. Every transition from one vertex in the assignment simplex to another is equally penalized with a

value of 2. By contrast, the new label space total variation model (L-TV) penalizes the total variation in the label space \mathcal{S} . Consequently, every transition from one vertex in the assignment simplex to another has a cost proportional to the geodesic distance between the corresponding labels on the sphere.

While (L-TV) appears natural, it is computationally more challenging to solve than (A-TV). This is due to the fact that the labels are situated in a nonlinear space (the sphere), and the evaluation of their mixture requires a Riemannian center of mass problem to be solved on each triangle as part of the optimization process. Future work should address opportunities to accelerate the associated Riemannian center of mass subproblem; see Section 4.2.4.

We observed that (A-TV) does not necessarily use all available labels, especially for large values of the regularization parameter. In particular, this can be observed in regions of constant curvature and multiple labels available for this region. In contrast, the proposed model (L-TV) utilizes more of the available labels. It also turns out to be more robust w.r.t. the choice of the regularization parameter β .

REFERENCES

- Alnæs, M.; J. Blechta; J. Hake; A. Johansson; B. Kehlet; A. Logg; C. Richardson; J. Ring; M. E. Rognes; G. N. Wells (2015). “The FEniCS project version 1.5”. *Archive of Numerical Software* 3.100, pp. 9–23. DOI: [10.11588/ans.2015.100.20553](https://doi.org/10.11588/ans.2015.100.20553).
- Åström, F.; S. Petra; B. Schmitzer; C. Schnörr (2017). “Image labeling by assignment”. *Journal of Mathematical Imaging and Vision* 58.2, pp. 211–238. DOI: [10.1007/s10851-016-0702-4](https://doi.org/10.1007/s10851-016-0702-4).
- Bergmann, R.; M. Herrmann; R. Herzog; S. Schmidt; J. Vidal-Núñez (2020a). “Discrete total variation of the normal vector field as shape prior with applications in geometric inverse problems”. *Inverse Problems* 36.5, p. 054003. DOI: [10.1088/1361-6420/ab6d5c](https://doi.org/10.1088/1361-6420/ab6d5c). arXiv: [1908.07916](https://arxiv.org/abs/1908.07916).
- Bergmann, R.; M. Herrmann; R. Herzog; S. Schmidt; J. Vidal-Núñez (2020b). “Total variation of the normal vector field as shape prior”. *Inverse Problems* 36.5, p. 054004. DOI: [10.1088/1361-6420/ab6d5b](https://doi.org/10.1088/1361-6420/ab6d5b). arXiv: [1902.07240](https://arxiv.org/abs/1902.07240).
- Boumal, N. (2023). *An Introduction to Optimization on Smooth Manifolds*. Cambridge University Press. DOI: [10.1017/9781009166164](https://doi.org/10.1017/9781009166164). URL: <https://www.nicolasboumal.net/book>.
- Boyd, S.; N. Parikh; E. Chu; B. Peleato; J. Eckstein (2010). “Distributed optimization and statistical learning via the alternating direction method of multipliers”. *Foundations and Trends in Machine Learning* 3.1, pp. 1–122. DOI: [10.1561/22000000016](https://doi.org/10.1561/22000000016).
- Chambolle, A.; T. Pock (2011). “A first-order primal-dual algorithm for convex problems with applications to imaging”. *Journal of Mathematical Imaging and Vision* 40.1, pp. 120–145. DOI: [10.1007/s10851-010-0251-1](https://doi.org/10.1007/s10851-010-0251-1).
- Charles, R. Q.; H. Su; M. Kaichun; L. J. Guibas (2017). “PointNet: deep learning on point sets for 3D classification and segmentation”. *2017 IEEE Conference on Computer Vision and Pattern Recognition (CVPR)*. IEEE, pp. 77–85. DOI: [10.1109/cvpr.2017.16](https://doi.org/10.1109/cvpr.2017.16).
- Cohen-Steiner, D.; P. Alliez; M. Desbrun (2004). “Variational shape approximation”. *ACM Transactions on Graphics* 23.3, pp. 905–914. DOI: [10.1145/1015706.1015817](https://doi.org/10.1145/1015706.1015817).

- Gauthier, S.; W. Puech; R. Bénére; G. Subsol (2017). “Digitized 3D mesh segmentation based on curvature analysis”. *Electronic Imaging* 29.20, pp. 33–38. DOI: [10.2352/issn.2470-1173.2017.20.3dipm-005](https://doi.org/10.2352/issn.2470-1173.2017.20.3dipm-005).
- Goldstein, T.; S. Osher (2009). “The split Bregman method for L_1 -regularized problems”. *SIAM Journal on Imaging Sciences* 2.2, pp. 323–343. DOI: [10.1137/080725891](https://doi.org/10.1137/080725891).
- González, A. (2009). “Measurement of areas on a sphere using Fibonacci and latitude-longitude lattices”. *Mathematical Geosciences* 42.1, pp. 49–64. DOI: [10.1007/s11004-009-9257-x](https://doi.org/10.1007/s11004-009-9257-x).
- Goto, J.; H. Sato (2021). “Approximated logarithmic maps on Riemannian manifolds and their applications”. *JSIAM Letters* 13, pp. 17–20. DOI: [10.14495/jsiaml.13.17](https://doi.org/10.14495/jsiaml.13.17).
- Hanocka, R.; A. Hertz; N. Fish; R. Giryes; S. Fleishman; D. Cohen-Or (2019). “MeshCNN: a network with an edge”. *ACM Transactions on Graphics* 38.4, pp. 1–12. DOI: [10.1145/3306346.3322959](https://doi.org/10.1145/3306346.3322959).
- He, Y.; M. Yousuff Hussaini; J. Ma; B. Shafei; G. Steidl (2012). “A new fuzzy c-means method with total variation regularization for segmentation of images with noisy and incomplete data”. *Pattern Recognition* 45.9, pp. 3463–3471. DOI: [10.1016/j.patcog.2012.03.009](https://doi.org/10.1016/j.patcog.2012.03.009).
- Hoppe, H.; T. DeRose; T. Duchamp; M. Halstead; H. Jin; J. McDonald; J. Schweitzer; W. Stuetzle (1994). “Piecewise smooth surface reconstruction”. *Proceedings of the 21st Annual Conference on Computer Graphics and Interactive Techniques - SIGGRAPH '94*. ACM Press, pp. 295–302. DOI: [10.1145/192161.192233](https://doi.org/10.1145/192161.192233).
- Hwan Kim, D.; I. Dong Yun; S. Uk Lee (2006). “Boundary-trimmed 3D triangular mesh segmentation based on iterative merging strategy”. *Pattern Recognition* 39.5, pp. 827–838. DOI: [10.1016/j.patcog.2005.11.022](https://doi.org/10.1016/j.patcog.2005.11.022).
- Karcher, H. (1977). “Riemannian center of mass and mollifier smoothing”. *Communications on Pure and Applied Mathematics* 30.5, pp. 509–541. DOI: [10.1002/cpa.3160300502](https://doi.org/10.1002/cpa.3160300502).
- Lellmann, J.; J. Kappes; J. Yuan; F. Becker; C. Schnörr (2009). “Convex multi-class image labeling by simplex-constrained total variation”. *Lecture Notes in Computer Science*. Springer Berlin Heidelberg, pp. 150–162. DOI: [10.1007/978-3-642-02256-2_13](https://doi.org/10.1007/978-3-642-02256-2_13).
- Lellmann, J.; C. Schnörr (2011). “Continuous multiclass labeling approaches and algorithms”. *SIAM Journal on Imaging Sciences* 4.4, pp. 1049–1096. DOI: [10.1137/100805844](https://doi.org/10.1137/100805844).
- Lellmann, J.; E. Strelakovski; S. Koetter; D. Cremers (2013). “Total variation regularization for functions with values in a manifold”. *2013 IEEE International Conference on Computer Vision*, pp. 2944–2951. DOI: [10.1109/ICCV.2013.366](https://doi.org/10.1109/ICCV.2013.366).
- Mumford, D.; J. Shah (1989). “Optimal approximations by piecewise smooth functions and associated variational problems”. *Communications on Pure and Applied Mathematics* 42.5, pp. 577–685. DOI: [10.1002/cpa.3160420503](https://doi.org/10.1002/cpa.3160420503).
- Nabi, H.; A. Douik (2016). “An extended Mumford-Shah model for shape partitioning”. *International Journal of Signal and Imaging Systems Engineering* 9.4/5, p. 226. DOI: [10.1504/ijssise.2016.078263](https://doi.org/10.1504/ijssise.2016.078263).
- Pock, T.; D. Cremers; H. Bischof; A. Chambolle (2009). “An algorithm for minimizing the Mumford-Shah functional”. *2009 IEEE 12th International Conference on Computer Vision*. IEEE, pp. 1133–1140. DOI: [10.1109/iccv.2009.5459348](https://doi.org/10.1109/iccv.2009.5459348).

- Shedelbower, A. (2022). *Sample 3D Model: Fan Disk*. Wolfram Data Repository. URL: <https://datarepository.wolframcloud.com/resources/Sample-3D-Model-Fan-Disk/> (visited on 05/17/2023).
- Stellato, B.; G. Banjac; P. Goulart; A. Bemporad; S. Boyd (2020). “OSQP: an operator splitting solver for quadratic programs”. *Mathematical Programming Computation* 12.4, pp. 637–672. DOI: [10.1007/s12532-020-00179-2](https://doi.org/10.1007/s12532-020-00179-2).
- Sun, Z.; R. Harik; S. Baek (2018). “Mesh segmentation via geodesic curvature flow”. *Computer-Aided Design and Applications* 15.5, pp. 677–683. DOI: [10.1080/16864360.2018.1441235](https://doi.org/10.1080/16864360.2018.1441235).
- Wang, J.; Z. Yu (2011). “Surface feature based mesh segmentation”. *Computers & Graphics* 35.3, pp. 661–667. DOI: [10.1016/j.cag.2011.03.016](https://doi.org/10.1016/j.cag.2011.03.016).
- Wang, W.; M. Á. Carreira-Perpiñán (2013). *Projection onto the probability simplex: an efficient algorithm with a simple proof, and an application*. arXiv: [1309.1541](https://arxiv.org/abs/1309.1541).
- Yamauchi, H.; S. Gumhold; R. Zayer; H.-P. Seidel (2005). “Mesh segmentation driven by Gaussian curvature”. *The Visual Computer* 21.8–10, pp. 659–668. DOI: [10.1007/s00371-005-0319-x](https://doi.org/10.1007/s00371-005-0319-x).
- Yan, D.-M.; W. Wang; Y. Liu; Z. Yang (2012). “Variational mesh segmentation via quadric surface fitting”. *Computer-Aided Design* 44.11, pp. 1072–1082. DOI: [10.1016/j.cad.2012.04.005](https://doi.org/10.1016/j.cad.2012.04.005).
- Zhang, J.; J. Zheng; C. Wu; J. Cai (2012). “Variational mesh decomposition”. *ACM Transactions on Graphics* 31.3, pp. 1–14. DOI: [10.1145/2167076.2167079](https://doi.org/10.1145/2167076.2167079).
- (L. Baumgärtner) INSTITUT FÜR MATHEMATIK, HUMBOLDT UNIVERSITY OF BERLIN, 10099 BERLIN, GERMANY
Email address: lukas.baumgaertner@hu-berlin.de
URL: <https://www.mathematik.hu-berlin.de/en/people/mem-vz/1693318>
- (R. Bergmann) NORWEGIAN UNIVERSITY OF SCIENCE AND TECHNOLOGY, DEPARTMENT OF MATHEMATICAL SCIENCES, NO-7041 TRONDHEIM, NORWAY
Email address: ronny.bergmann@ntnu.no
URL: <https://www.ntnu.edu/employees/ronny.bergmann>
- (R. Herzog) INTERDISCIPLINARY CENTER FOR SCIENTIFIC COMPUTING, HEIDELBERG UNIVERSITY, 69120 HEIDELBERG, GERMANY
Email address: roland.herzog@iwr.uni-heidelberg.de
URL: <https://scoop.iwr.uni-heidelberg.de>
- (S. Schmidt) UNIVERSITY OF TRIER, UNIVERSITÄTSRING 15, 54296 TRIER, GERMANY
Email address: s.schmidt@uni-trier.de
URL: <https://www.math.uni-trier.de/~schmidt>
- (M. Weiß) INTERDISCIPLINARY CENTER FOR SCIENTIFIC COMPUTING, HEIDELBERG UNIVERSITY, 69120 HEIDELBERG, GERMANY
Email address: manuel.weiss@iwr.uni-heidelberg.de
URL: <https://scoop.iwr.uni-heidelberg.de>